Realization of a Multi-Pole Permanent Magnetic Bearing with Rotating Magnetization

Edmund Marth[a], Gerald Jungmayr[a], Jörg Kobleder[a], Martin Panholzer[a] and Wolfgang Amrhein[a]

[a] Department of Electrical Drives and Power Electronics, Johannes Kepler University, Altenbergerstrasse 69, 4040 Linz, Austria, edmund.marth@jku.at

***Abstract*—The optimization of stiffness of a permanent magnetic single ring bearing is presented in this paper. This is achieved by only changing the magnetization pattern. More precisely, a homogeneous magnetization is replaced by a rotating magnetization with two magnetic poles, leading to a 3.7-fold improvement in stiffness. Usually, such a rotating magnetization is realized by stacking several homogeneously magnetized rings with different magnetization direction, which is referred to as Halbach stacking. Our approach was to realize a continuously rotating magnetization pattern in one ring. In order to achieve the maximum possible stiffness for the given bearing dimensions, the optimization of the magnetization process is crucial and also presented in the paper.**

I. Introduction

For the design of permanent magnetic ring bearings guidelines are available which help to obtain a bearing with a high functional value, i.e., stiffness or force, with respect to the volume of the permanent magnetic rings. This objective is crucial since the total volume of the magnetic material is directly linked to the costs of the final bearing. The possible design variables are the geometrical dimensions, the number of magnetic poles, and the shape of the magnetization. How these parameters influence the stiffness or force value of the resulting bearing is described in several publications, e.g., [1]–[5]. In summary, a "good" bearing should have cross section dimensions (per magnetic pole) in the size of the air gap, at least three magnetic poles, and a rotating magnetization. As shown in [5] the optimal cross section dimensions, in terms of maximal stiffness per magnet volume, are often unrealistic. Either the necessary geometric dimensions are too small to be fabricated or the absolute stiffness value is too low (see [5] for detailed information). Concerning the rotating magnetization there are basically two methods for realization: (i) several permanent magnet rings with homogeneous, but in its direction rotating magnetization can be stacked together or (ii) one permanent magnet ring is magnetized to reach a continuously rotating magnetization, cf. [1], [4]. Such magnetization patterns are also referred to as Halbach stacking or continuous Halbach magnetization respectively. What we present in this paper is the realization of such a multi-pole bearing with continuously rotating magnetization. As the bearing should replace a standard bearing used in an existing permanent magnetic levitated system, the geometric dimensions of the bearing are predefined. Thus, the paper basically deals with the maximization of the radial stiffness by means of an optimized magnetization pattern. This also includes the optimization of the necessary magnetization coil as well as the magnetization process.

Basic configurations of permanent magnetic bearings with continuously rotating magnetization are shown in Fig. 1(a) and (b) in attractive and repulsive configuration respectively. The

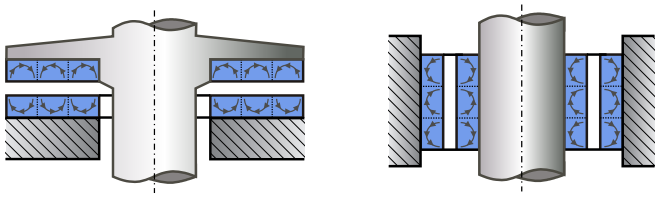

(a) attractive (b) repulsive

Figure 1: Exemplary configurations of radially stable bearings with three magnetic poles and continuous Halbach magnetization.

single ring bearing with homogeneous magnetization shown in Fig. 2 is the starting point for optimization. The corresponding parameters are given in Table I. The permanent magnetic

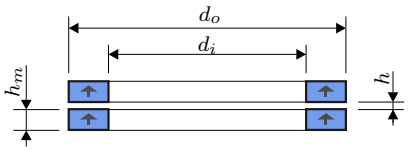

Figure 2: Configuration which is to be optimized with respect to maximum stiffness.

Table I: Geometric parameters of the attractive bearing to be realized

Parameter	Value	Description
d_i	21 mm	inner diameter
d_o	29 mm	outer diameter
h_m	2.2 mm	axial height of one magnet
h	0.7 mm	axial air gap of the bearing

material used for the realization is an isotropic ferrite. The characteristic parameters are summarized in Table II.

Table II: Permanent magnetic material data, measured at 24°C

Parameter	Value	Parameter	Value
B_r	0.208 T	$H_{c,B}$	$-147\,\mathrm{kA/m}$
$H_{c,J}$	$-279\,\mathrm{kA/m}$	$(BH)_{max}$	$7.8\,\mathrm{kJ/m^3}$
μ_r	1.13		

II. Magnetization of the Annular Rings

A. Magnetization Coil

To obtain a continuous rotating magnetization for bearings in attractive configuration the necessary arrangement of the magnetization coils with the proper current direction is shown in Fig. 3. That the number of coils n_c can be higher than the number of magnetic poles p is an additional degree of freedom for optimization. This might be advantageous for minimizing edge effects. To ensure full magnetization of the permanent

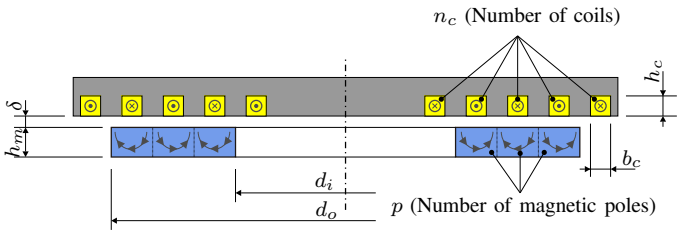

Figure 3: Parametric model of the magnetization coil.

magnet, the magnetic field generated by the coils has to be roughly the triple coercitivity of the polarization $H_{c,J}$, about $840\,\mathrm{kA/m}$ in our case. Since a sinusoidal magnetization is desired, cf. [4], [5], no iron can be used for flux guiding. As a consequence, very high currents are necessary to obtain this flux density. Hence, the temperature of the coils will rise significantly, which is the limiting factor in the design of the magnetization coil.

B. Magnetization Current and Thermal Behavior

The equivalent circuit for the simulation of the magnetization current is shown in Fig. 4 and includes the magnetization coil and the magnetizer used to energize the coil. The magnetizer is an impulse magnetizer manufactured by the

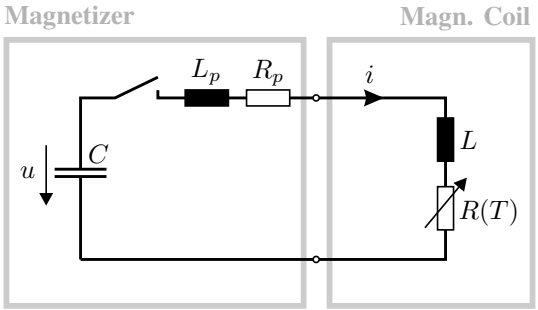

Figure 4: Equivalent circuit for the magnetization process, including magnetization coil and magnetization stage.

mPulse company[1]. The important ratings are given in Table III. The values of the parasitic parameters R_p and L_p where identified from prior measurements. Since the magnetization

Table III: Magnetizer ratings

Parameter	Value	Comment
$U_{C,0}$	up to 3000 V	continuously adjustable; $U_{C,0} = u_{(t=0)}$
C	fix: $540\,\mu$F $2 \times 810\,\mu$F $4 \times 1080\,\mu$F	arbitrary combination possible; $C = 540\,\mu$F up to $6480\,\mu$F
i_{max}	50 kA	maximum output current
W_{max}	29, 16 kJ	maximum magnetization energy
R_p	$14\,\mathrm{m\Omega}$	identified parasitic resistance
L_p	$2.5\,\mu$H	identified parasitic inductivity

current i can not be arbitrarily big due to thermal reasons, the coil temperature T has to be modeled by defining the ohmic resistance of the coil as function of the temperature:

$$R(T) = R_{20} \cdot (1 + \alpha \cdot \Delta T) \ . \tag{1}$$

Here, ΔT is $T - 20°\mathrm{C}$, R_{20} denotes the resistance at room temperature (20°C), and α denotes the temperature coefficient of copper. The ohmic resistance of the coil at room temperature can be calculated by

$$R_{20} = \rho \cdot \frac{l}{A} \tag{2}$$

with the specific resistance of copper ρ, the total length l of all n_c coils, and the cross section area per single coil $A = b_c \cdot h_c$.

The thermal energy E_{th} stored in the copper of the coil is

$$E_{th} = c_p \cdot m \cdot T_K \ ,$$

where m is the mass of the coil, c_p the specific heat capacity of copper and T_K the absolute temperature of the coil in Kelvin. Assuming, that the total thermal energy E_{th} of one single magnetizing event is stored in the copper, i.e., no energy is emitted by heat transfer, radiation or convection, one can calculate the increase of the coil temperature via

$$\mathrm{d}E_{th} = R(T) \cdot i^2 \mathrm{d}t \ ,$$
$$\frac{\mathrm{d}E_{th}}{\mathrm{d}t} = c_p \cdot m \frac{\mathrm{d}T_K}{\mathrm{d}t} = R(T) \cdot i^2$$

and finally

$$\dot{T} = \frac{R(T) \cdot i^2}{c_p \cdot m} \ . \tag{3}$$

Since only a temperature gradient is calculated in (3), the absolute temperature T_K is substituted by the temperature in degrees Celsius, T. Although equation (3) gives a worst case estimation, pratical results are expected to be close due to the short period while the coil is energized, cf. Fig. 5. The final state equations describing the dynamic behavior of the magnetization current i and the Temperature of the copper are

$$\dot{u} = \frac{i}{C} \tag{4}$$

$$\dot{i} = \frac{u - i \cdot (R_{20} \cdot (1 + \alpha_{20} \cdot \Delta T) + R_p)}{L + L_p} \tag{5}$$

$$\dot{T} = \frac{i^2 \cdot R_{20}(1 + \alpha_{20} \cdot \Delta T)}{c_p \cdot m} \ . \tag{6}$$

[1] www.m-pulse.biz

All parameters used in equations (1) to (6) are summarized in Table IV. The coil inductivity L was calculated with the

Table IV: Parameters of the magnetization-current simulation

Parameter	Value/Unit	Comment
α	$3.9 \cdot 10^{-3}\,\mathrm{K}^{-1}$	temperature coefficient of resistance of copper
c_p	$384\,\frac{\mathrm{J}}{\mathrm{kgK}}$	specific heat capacity of copper
ρ	$17.8 \cdot 10^{-9}\,\Omega\mathrm{m}$	specific resistance at 20°C
$i(t)$	A	magnetization current, state variable
$u(t)$	V	voltage drop over C, state variable
$T(t)$	°C	coil temperature, state variable
$R(T)$	Ω	coil resistance, function of the geometric design parameters
R_{20}	Ω	coil resistance at 20°C, function of the geometric design parameters
L	H	coil inductivity, function of the geometric design parameters

FEMM finite element software[2], based on the given geometric parameters and the number of coils n_c. As an additional parameter, each coil can have N windings. The resistance was also calculated as function of the geometric parameters, n_c, and N. Furthermore, an estimated value of the resistance representing the supply wires and the interconnections of the single coils was added.

The simulated magnetization current and the simulated coil temperature are shown in Fig. 5 together with the measured magnetization current. The measurement was done with the configuration built up and which is described in detail in the realization section III-C. Fig. 5 shows that the derived model is well suited to predict the magnetization current.

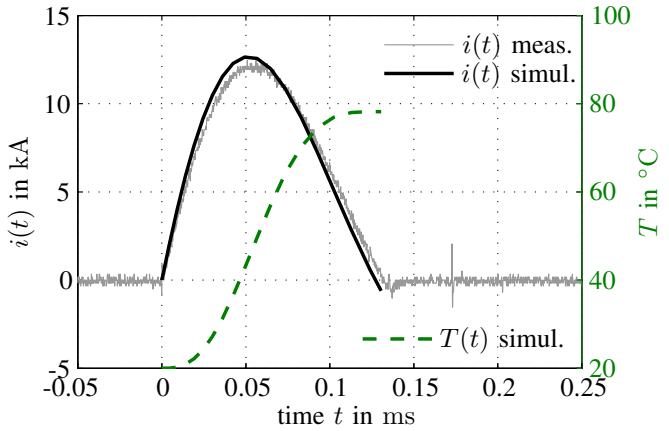

Figure 5: Magnetization current and coil temperature during one energizing process, simulation and measurement.

III. Optimization of the Magnetizing Process

A. Optimization Problem Formulation

As mentioned, the main goal of this optimization is to maximize the radial stiffness of a bearing with given cross section dimensions by adapting the magnetization pattern. The bearing we want to optimize is pictured to scale in Fig. 2 and its dimensions are given in Table I. Due to the available magnetizer and the thermal constraints, the whole magnetization process, as presented in the previous section, has to be considered in such an optimization. The available design parameters with the allowed range of values are defined in Table V. Objectives and constraints of the optimization

Table V: Design variables for the optimization

Parameter	Min.	Max.	Unit	Comment
δ	0.1	2	mm	
h_c	0.5	5	mm	
p	1	4		$p \in \mathbb{N}$
x_{b_c}	0.1	0.8		$b_c = x_{b_c} \cdot \frac{d_o - d_i}{2p}$
n_c	p	$p+8$		$n_c \in \mathbb{N}$
N	1	10		$N \in \mathbb{N}$
$U_{C,0}$	100	3000	V	
C	540	6480	μF	$C \in \{540, 1350, 2160, 3240, 4320, 5400, 6480\}\mu$F

are given in Table VI. For the temperature T it is clear that it should be minimal. In order to reduce the solution space to a feasible region, an upper constraint of $T = 250\,°\mathrm{C}$ was defined. The peak value of the magnetization current $\hat{i}$ is no objective, but again an upper limit is defined due to the limitations of the magnetizer. Instead of maximizing the radial stiffness of the bearing the negative axial stiffness $-k_z$ is maximized. The advantage of this objective is, that the axial stiffness can be calculated with a two dimensional finite element program due to the rotational symmetry, whereas the calculation of the radial stiffness represents a three dimensional problem which would lead to a highly increased time used for optimization. This approach is valid, because the axial stiffness is directly linked to the radial stiffness by the so called Earnshaw Theorem, ([6], [7]). Earnshaws Theorem states that if no magnetically conducting material is involved and $\mu_r = 1$ also for the magnets,

$$k_z = -2 \cdot k_r \tag{7}$$

holds true. Even if Earnshaw's assumptions are not perfectly fulfilled, ($\mu_r = 1.13$!), maximization of $-k_z$ will lead to high radial stiffness.

Table VI: Objectives and constraints

		Constraints		
Parameter	Objective	Min.	Max.	Unit
$-k_z$	maximized			N/mm
T	minimized	–	250	°C
$\hat{i}$	no Obj.	–	50	kA

B. Optimizing using MagOpt

For the optimization of this multi objective problem the software tool MagOpt (short for Magnetic Optimization[3]) is

[2] www.femm.info

[3] It should be noted, that the tool has a very general structure and thus is not limited to magnetic problems.

used [8]. It is developed at the Department of Electrical Drives and Power Electronics and the Linz Center of Mechatronics and is designed to serve as a kind of communication- or interface manager. In MagOpt, which is implemented in the Java programming language, the whole optimization project can be set up in the form of a tree structure, allowing to link different simulation-, calculation-, and CAD-software with each other. MagOpt is capable of checking all dependencies within the project and consequently executing the whole tree in the proper order. Furthermore, MagOpt has a built in optimization tool using genetic algorithms, which was used for this optimization. Let us look at our problem, also to clarify MagOpt's working principle.

In order to find the optimal solution, we first have to generate an initial parameter set (cf. Table V). When using genetic algorithms, such a set of design parameters is called an individual. Typically hundreds of such individuals with different parameter sets form a generation and are preferably processed in parallel. The following description is also visualized in Fig. 6 and explains the processing of one individual.

The design parameters are defined as so called "parameter fields" within the MagOpt tree[4]. These parameters can now act as an input for any function defined in the tree. For example, solving our problem requires the calculation of the magnetization coils' inductivity. This is done, as mentioned earlier, by involving the finite element software FEMM, which receives all relevant parameters from MagOpt. After calculation is finished, MagOpt collects the results from the FEMM output and makes them available within the MagOpt tree for further processing. As simple algebraic equations can be solved directly within MagOpt, the total resistance of the magnetization coil can be determined. Thus, all necessary parameters to simulate the magnetization current and the temperature of the coil can be committed to Matlab/Simulink, where equations (4) to (6) are implemented. The results of this simulation, namely the peak current $\hat{i}$ and the coil temperature T, are again collected by MagOpt. By applying $\hat{i}$ to the magnetization coil, the resulting magnetization pattern can be determined. Therefore, again in FEMM, the magnet is sectioned in lots of small elements. Each element is magnetized according to the strength and orientation of the magnetic field produced by the coil. To determine the strength of the permanent magnetic magnetization the initial magnetization curve pictured in Fig. 7 was used. To determine the axial stiffness of the whole bearing, this single ring is mirrored with reversed direction of magnetization and the axial force as function of axial displacement is calculated. The final magnetization pattern with the corresponding field lines and nominal air gap is shown in Fig. 8. The stiffness value is again collected by MagOpt.

Now the optimizer evaluates the results of all individuals, namely the objective values, and generates new datasets by combining the best individuals. A new generation is born and ready to be evaluated. All the steps and functionality performed by external programs such as FEMM are controlled mainly by script files, e.g., LUA-script for FEMM, which are also defined in MagOpt.

[4]This tree has the same structure for all individuals, but different parameter values.

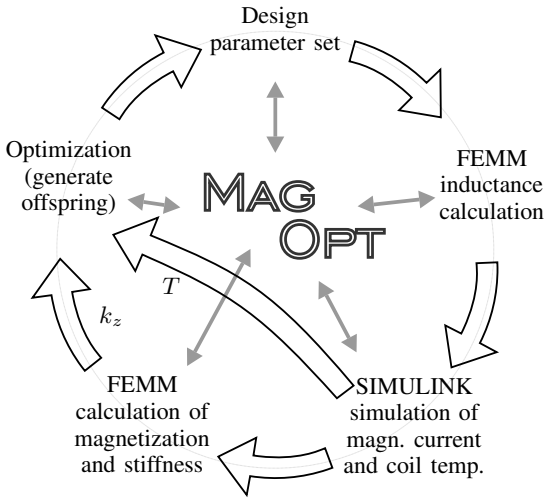

Figure 6: Optimization path

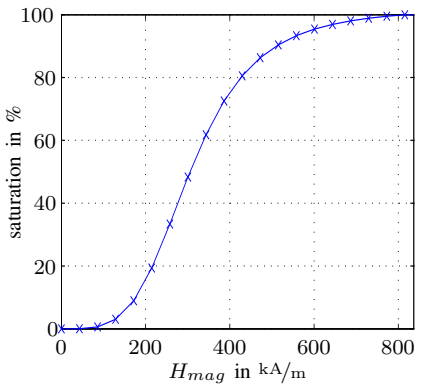

Figure 7: Assumed initial curve of the polarization's saturation used to determine the polarization in each section of the permanent magnet. Full magnetization is achieved for field strength $H_{mag} \geq 3 \cdot H_{c,J}$.

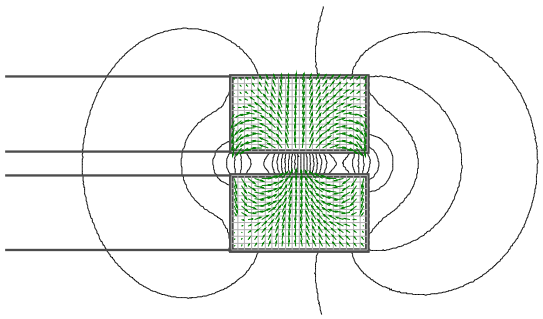

Figure 8: Calculated magnetization pattern and magnetic field lines of the realized bearing.

C. Pareto– optimal Solution and Realization of the Magnetization Coil

The outcome of the multi-objective optimization is the Pareto front shown in Fig. 9. The parameters of the chosen configuration are summarized in Table VII. The slight deviation from the Pareto optimal solution is due to the required discretization of the coils cross section area to fit available wire dimensions. In our case a $0.6 \times 1.3\,\mathrm{mm}$ wire is used.

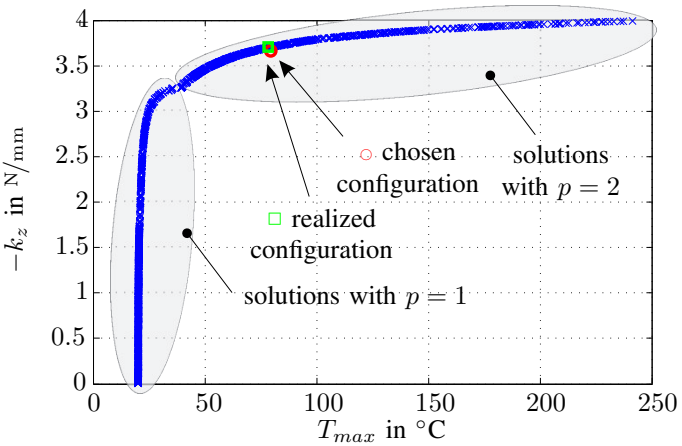

Figure 9: Pareto front showing axial stiffness vs. magnetization coil temperature.

Table VII: Selected configuration

Parameter	Value	Parameter	Value
	DESIGN PARAMETERS		
n_c	6	N	2
b_c	1.6 mm	h_c	1.3 mm
$U_{C,0}$	1200 V	C	540 μF
p	2	δ	0.1 mm
	OBJECTIVE VALUES AND SUBSIDIARY PARAMETERS		
$-k_z$	3.66 $^{\mathrm{N}}/_{\mathrm{mm}}$	T_{max}	79°C
L	319 nH	R_{20}	20.8 mΩ
i_{max}	11.8 kA	m	8.6 g

The realized magnetization coil is shown in Fig. 10. From the real setup, a slightly different resistance and mass was measured, leading to a necessary voltage of the magnetizer of $U_{C,0} = 1330V$ in order to reach a similar peak current and maximum coil temperature as gained from the optimization. The real parameters are the corresponding simulation results are listed in table VIII.

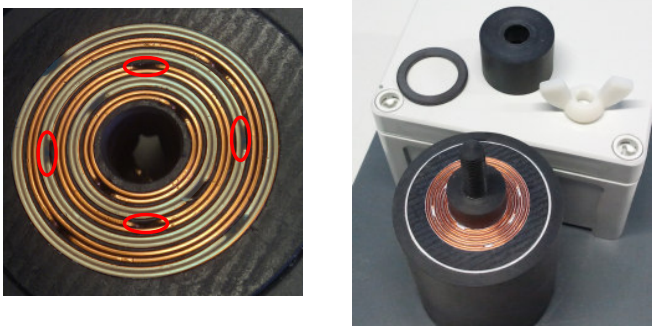

(a) (b)

Figure 10: Realized magnetization coil. (a) Detailed view on the realized magnetization coil; every second single coil is shaded for better distinction; observe the symmetric positioning of the threwholes – indicated by the small ovals – in order to minimize cogging effects. (b) Complete setup.

Table VIII: Deviating parameters of the realized configuration with respect to table VII

Parameter	Value	Parameter	Value
R_{20}	25 mΩ	m	12 g
$U_{C,0}$	1330 V	i_{max}	12.6 kA
$-k_z$	3.7 $^{\mathrm{N}}/_{\mathrm{mm}}$	T_{max}	78°C

The simulated magnetization current and the measured one has already been shown in Fig. 5. The data used for simulation corresponds to table VIII and the magnetizer was also initialized with $U_{C,0} = 1330\,\mathrm{V}$.

IV. FORCE MEASUREMENTS

For comparison and validation of the calculation methods used for the optimization, the force of the single ring bearing with axial magnetization was measured. The setup for the force measurements is pictured in Fig. 11. Since magnetization

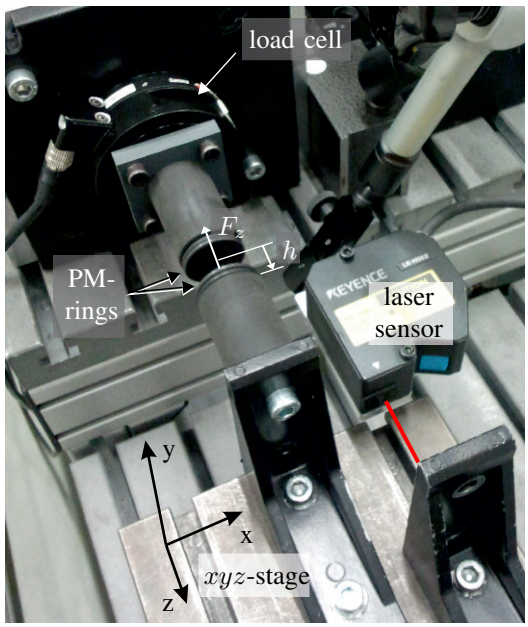

Figure 11: Setup to measure the axial force of permanent magnetic bearings. Force is measured by a load cell, the air gap distance is captured by a laser sensor.

in axial direction is easy to realize, full magnetization can be assumed within the whole volume of the magnet. The measured axial force as function of the air gap dimension h and the corresponding finite element calculation done with FEMM for the axially magnetized bearing are pictured in Fig. 12, showing a very good agreement. Furthermore, the force measurement is fitted by a polynomial and the stiffness is calculated therefrom by $k_{ax} = \frac{\mathrm{d}F_z}{\mathrm{d}h}$. Positive values of h an F_z point in the directions as indicated in Fig. 11.

Similar data is given for the realized bearing with rotating magnetization in Fig. 13. These results show a certain deviation between measured and calculated data. Possible reasons for this difference are: (i) the material is not isotropic, as assumed (the data from table II are measured only in axial

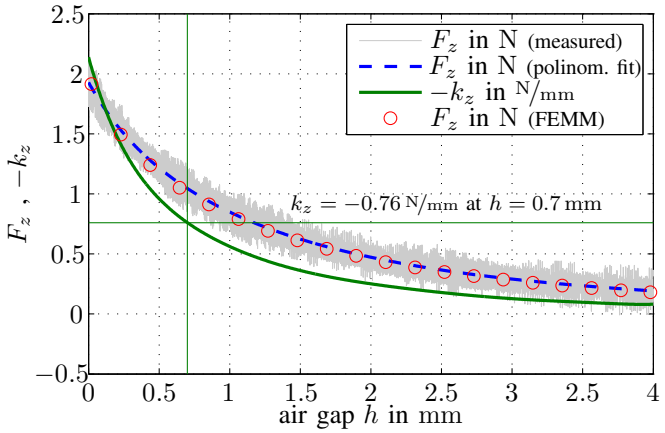

Figure 12: Axial force and stiffness value of the bearing with axial magnetization (cf. Fig. 2); the stiffness value is gained from the polynomial fit of the axial force.

direction) and/or (ii) the initial curve of the material, which we did not have at our disposal, was badly assumed (cf. Fig. 7). Unfortunately, these influences are hard to validate due to the lack of material data. That the (theoretically) desired peak current was reached during the magnetization process can be seen from Fig. 5. In this context it might be worth to be mentioned, that even bearings with peak currents during magnetization of up to 15 kA did not lead to improved results.

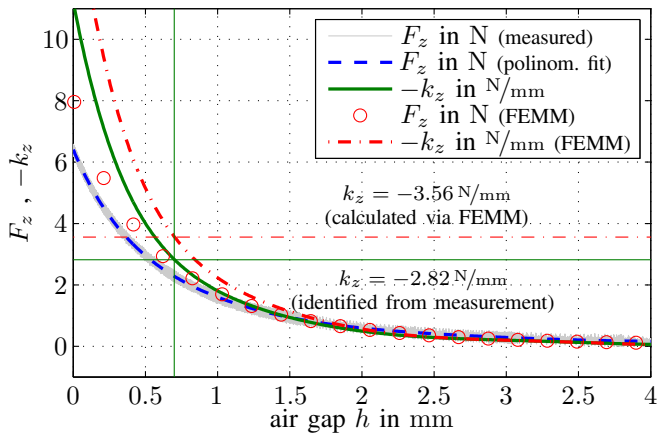

Figure 13: Axial force and stiffness value of the bearing with rotating magnetization (cf. Fig. 8); stiffness values are gained from polynomial fits of the axial forces (fit of FEMM-calculated force values are not shown).

Nevertheless, comparing the axially homogeneous magnetized bearing with the optimized one, a 3.7- fold improvement in the stiffness value and a 2.7- fold improvement in force value was achieved just by optimizing the magnetization pattern.

Concerning the stiffness calculation, the different values for k_z given in table VIII and Fig. 13 originate from a slightly different calculation method. During optimization the stiffness is calculated from the force values via the central differential quotient, while in Fig. 13 the stiffness is calculated from a polynomial fit of the calculated force values. This also points out the general problem of stiffness calculation via the finite element method.

Referring to [4], [5], the geometric parameters of the single ring bearing are very bad. But even compared to a standard double ring bearing as shown in Fig. 14, where a stiffness of $k_z = -1.8\,\mathrm{N/mm}$ and a force of $F_z = 1.4\,\mathrm{N}$ were calculated via FEMM, the improvement is still notable.

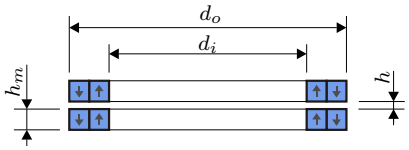

Figure 14: Bearing in double ring configuration; geometric parameters as given in table I.

Another interesting aspect can be seen from the magnetization pattern, Fig. 8. Due to the geometric specifications it was not possible to reach a rotating magnetization within the whole cross section of the magnets. In the outer regions the pattern resembles rather the initial axial magnetization than the rotating one. Thus, if the bearing is thought as a combination of two bearings as pictured in Fig. 15, the outer bearing has bad magnetization pattern and a big air gap. The contribution of the outer bearing to the total stiffness is therefore low compared to the magnet volume. For the inner bearing, the stiffness calculates to 77% of the value given in table VIII with only 50% of magnet volume.

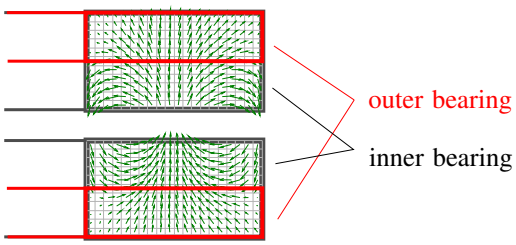

Figure 15: Conceptional configuration with two separate bearings.

The latter example of conceptionally splitting up the bearing is intended to show another possible issue of an optimized design and the importance of the proper geometric dimensions. In particular the strong correlation between the possible magnetization depth (in h_m direction) and the pole width $^{d_o-d_i}/_{2p}$ is a realization specific aspect to be considered. An advantage of the continuous rotating magnetization as presented in this paper is, that the number of poles not necessarily has to be an integer value. Looking at the Pareto front, Fig. 9, a rational number of poles leads to an improved Pareto front in the region between solutions with $p = 1$ and $p = 2$, i.e., in the region between $25°C < T_{max} < 75°C$.

V. Further Work

Concerning the deviation of calculation and measurement of the continuous Halbach bearing further investigations are

necessary. First of all, the anisotropic initial magnetization curves of the material are important in order to eliminate the possible errors mentioned.

VI. Conclusion

The presented work shows the possible improvement of stiffness and force values due to an optimized magnetization pattern. Also the importance of including the magnetization process itself becomes obvious.

Including the magnetization coil and the magnetization process in the bearing optimization is a novel approach for permanent magnetic bearing design. It represents the whole physical magnetization mechanism to reach maximum stiffness: the simulation of the magnetization current and coil temperature, the alignment of the elementary magnetic dipoles and the calculation of the stiffness of the final bearing.

Highly efficient designs can be expected if also the geometric parameters are adjusted during optimization.

VII. Acknowledgment

Parts of this work were supported by the Linz Center of Mechatronics (LCM) GmbH, a K2-center of the COMET program of the Austrian Government. The authors thank the Austrian and Upper Austrian Government for their support.

References

[1] J.-P. Yonnet, G. Lemarquand, S. Hemmerlin, and E. Olivier-Rulliere, "Stacked structures of passive magnetic bearings," *Journal of Applied Physics*, vol. 70, no. 10, pp. 6633–6635, November 1991.

[2] M. Lang and J. K. Fremerey, "Optimization of permanent-magnet bearings," in *6th International Symposium on Magnetic Suspension Technology*. Turin, Italy: Politecnico di Turino, October 2001. [Online]. Available: www.magneticbearings.org

[3] R. Moser, J. Sandtner, and H. Bleuler, "Optimization of repulsive passive magnetic bearings," *Magnetics, IEEE Transactions on*, vol. 42, no. 8, pp. 2038–2042, 2006.

[4] E. Marth, G. Jungmayr, M. Panholzer, and W. Amrhein, "Optimization of stiffness per magnet volume ratio of discrete and continuous Halbach type permanent magnetic bearings," in *ISMB13, 13th International Symposium on Magnetic Bearings*, 2012. [Online]. Available: www.magneticbearings.org

[5] E. Marth, G. Jungmayr, and W. Amrhein, "A 2-d-based analytical method for calculating permanent magnetic ring bearings with arbitrary magnetization and its application to optimal bearing design," *Magnetics, IEEE Transactions on*, vol. 50, no. 5, pp. 1–8, May 2014.

[6] S. Earnshaw, "On the nature of molecular forces wich regulate the constitution of luminiferous ether," *Transactions of the Cambridge Philosophical Society*, vol. 7, no. 1, pp. 97–112, 1842.

[7] W. Braunbeck, "Freischwebende Körper im elektrischen und magnetischen Feld," *Zeitschrift Physik*, vol. 112, pp. 753–763, 1939.

[8] S. Silber, W. Koppelstätter, G. Weidenholzer, and G. Bramerdorfer, "MagOpt – optimization tool for mechatronic components," in *Proceedings of the 14th International Symposium on Magnetic Bearings*, 2014. [Online]. Available: www.magneticbearings.org